Review

Analysis of Kinetic Curves of Mass Change During the Interaction of Active Gases with Certain Metals and Compounds with Simultaneous Evaporation of the Products of Reaction

Irakli Nakhutsrishvil *

Posted Date: 23 April 2024

doi: 10.20944/preprints202404.1442.v1

Keywords: Kinetics of oxidation; Scale evaporation; Mass change

 doi:10.20944/preprints202404.1442.v1

Review

Analysis of Kinetic Curves of Mass Change During the Interaction of Active Gases with Certain Metals and Compounds with Simultaneous Evaporation of the Products of Reaction

Irakli Nakhutsrishvili

Institute of Cybernetics of Georgian Technical University, 0186 Tbilisi, Georgia;
iraklinakhutsrishvili52@gmail.com

Abstract: The influence of the secondary process of evaporation of the reaction product on the kinetics of interaction of gases (O_2, Cl_2, NH_3, H_2O and N_2H_4 vapors) with the surface of some metals (Cr, Pb, Si, Ge) and compounds (BN, SiO_2, SiC) is discussed. Also is considered the case when the growth of the scale is preceded by the process of gas etching of the metal surface. A general equation is given that describes the scale growth-evaporation kinetic (sample mass change - time) curves during the interaction of gases with the surface of metals and compounds. Special cases of parabolic, cubic and fourth degree processes are discussed.

Keywords: kinetics of oxidation; scale evaporation; mass change

1. Introduction

This work is a continuation of [1], where the role of reduction of the reaction surface and evaporation of scale in the process of oxidation of FeCr and FeCrAl alloys is considered. Here we will consider in more detail the influence of the secondary process of evaporation (sublimation) on the formal kinetics (mass change - time) of the interaction of gases (O_2, Cl_2, NH_3, H_2O and N_2H_4 vapors) with some metals and compounds. We used data from various works collected in [2], the results of the indicated author, as well as your data.

The process of scale formation with simultaneous evaporation is called the Tedmon's process [3] (althoug such cases were discussed a little earlier [4,5]). This model is used when the overall kinetics is determined by the diffusion of ions in the scale (volume diffusion) rather than by the rate of the chemical reaction itself. In this case, the kinetics is parabolic [6–13]. With short-circuit diffusion, cubic kinetics takes place [6–11], and in the case of local electric fields and space charges, the kinetic law of the fourth degree is implemented. Kinetic data with the latter mechanism are also presented in number of works [6,7,17,18].

All of the above is clearly shown in the kinetic dependences of the mass gain, when the following happens: the mass of the sample first monotonically increases with deceleration, reaches a maximum, and then, when the rates of growth and evaporation are equalized, begins to decrease (Figure 1). Here, curve 1 shows the total mass change (M) of the metal-scale system, and curve 2, plotted graphically on its basis (excluding the contribution of evaporation), corresponds to the increase of mass (m) due to the reacted gas: $m=M+v_m t$, where v_m is the evaporation rate to the metal component of the scale, t is the time. The section OA (OA_1) corresponds to the gradual growth of scale, and the straight section AB (A_1B_1) corresponds to the stationary regime, when the amounts of the formed and evaporating products are equalized (the first gradually decreases due to diffusion limitation, while the second is constant in an isothermal process). In this case, the layer reaches its maximum mass (thickness). The slope of the straight line AB corresponds to the rate of the mass decrease of the sample: $v_m=-tg\beta$. (Here we consider the coordinate systems t - m and t - M; the coordinate system t_W – W is considered further.)

Preprints.org (www.preprints.org) | NOT PEER-REVIEWED | Posted: 23 April 2024 doi:10.20944/preprints202404.1442.v1

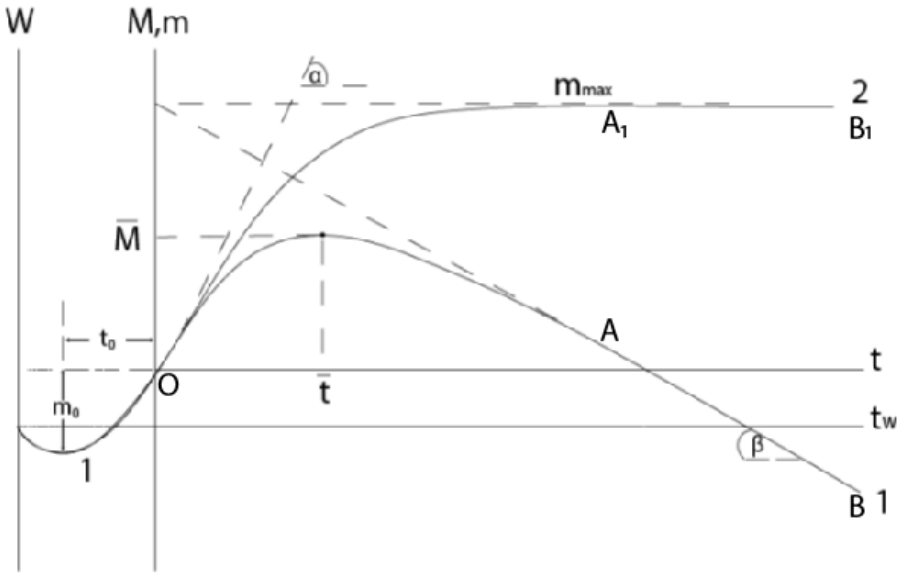

Figure 1. Schematic representation of the kinetic curves of the total mass change (1) and its increase due to the reacted gas (2); ($\bar{t}$,$\bar{M}$) – coordinates of M_{max}.

The rate of mass increase due to the reacted gas in the general case is:

$$\frac{dm}{dt} = \frac{k_n/n}{m^{n-1}+(k_n/nr_r)} - v_g, \quad (1)$$

where n=2, 3 or 4; $k_r \equiv dm/dt$ (at point t=0,m=0)=tgα is rectilinear constant; k_n is the power-law constant; v_g is the speed of the system mass reduction due to the gas component of the evaporating part of the scale. Its integral form is as follows:

$$t=(1+k)\frac{m_{max}^{n-1}}{v_g}\int \frac{dm}{m_{max}^{n-1}-m^{n-1}} - \frac{m}{v_g}, \quad (2)$$

where $k=v_g/(k_r - v_g)$, $m_{max} = (k_n/nk_rk)^{1/(n-1)}$ is the maximum mass gain of the system at the expense of active gas.

Boundary condition for solving of Eq.(2) for different n: t=0,m=0.

The Tedmon-Wajsel equation (n=2) in our notation will be:

$$t=-(1+k)\frac{m_{max}}{v_g}\ln\frac{m_{max}-m}{m_{max}} - \frac{m}{v_g}. \quad (3)$$

For n=3 and 4 we will have:

$$t=(1+k)\frac{m_{max}}{2v_g}\ln\frac{m_{max}+m}{m_{max}-m} - \frac{m}{v_g}, \quad (4)$$

$$t=(1+k)\frac{m_{max}}{v_g}\left[\frac{1}{\sqrt{3}}\text{arctg}\frac{\sqrt{3}m}{m+2m_{max}} - \frac{1}{6}\ln\frac{(m_{max}-m)^2}{m^2+mm_{max}+m_{max}^2}\right] - \frac{m}{v_g}, \quad (5)$$

respectively [17]. For the total mass change will be:

$$M=m-v_mt. \quad (6)$$

Such containing maxima curves were obtained in a number of works [19–29] and works collected in [2]. Here we will look at graphs in which this maximum is clearly expressed and from which reliable information can be obtained (some graphs, which are not considered here, give unrealistic values of kinetic parameters).

 doi:10.20944/preprints202404.1442.v1

2. Discussion

2.1. Kinetic Curves of the Total Mass Change, Having a Maximum

As mentioned above, kinetic curves containing a maximum are presented in many works. Most of them are curves corresponding to parabolic kinetics (n=2); there is little data for n=4; but for n=3 we did not find such data (if we do not consider the curve presented in Figure 4a), although cubic processes (with curves without maxima) are considered in a fairly large number of works.

Figure 2 shows the data of [20,21]. To determine n, we can use the formula [17]:

$$n=\frac{\lg[(1-qk)(\overline{M}+v_m\bar{t})/pm_{max}]}{\lg[(\overline{M}+v_m\bar{t})/m_{max}]}, \quad (7)$$

where $q=v_m/v_g$, $p=(v_m+v_g)/v_g=q+1$. The tangents of the curves in Figure 2 virtually coincide with ordinate axis at the origin of the coordinates: $k_r \to \infty \Rightarrow k \to 0$. In this case formula (7) is simplified as follows:

$$n=\frac{\lg[(\overline{M}+v_m t)/pm_{max}]}{\lg[(\overline{M}+v_m t)/m_{max}]}. \quad (8)$$

According to formula (8) for [21] it turns out n≅2.02, and for [20] n≅3.75, that are approaching to 2 and 4. Corresponding empirical expressions are: $t \cong -15.707\ln(1-0.554m) - 8.693m$ and $t \cong 28.885\{[0.577\,\mathrm{arctg}((1.424m)/(0.822m+2)] - [0.167\ln((1-0.822m)^2/(m^2+0.822m+1))]\}$--23.75m, where m is in mg/cm² and t is in hours. The curves constructed using these equations on the scale used in Figure 2 practically coincide with the experimental curves.

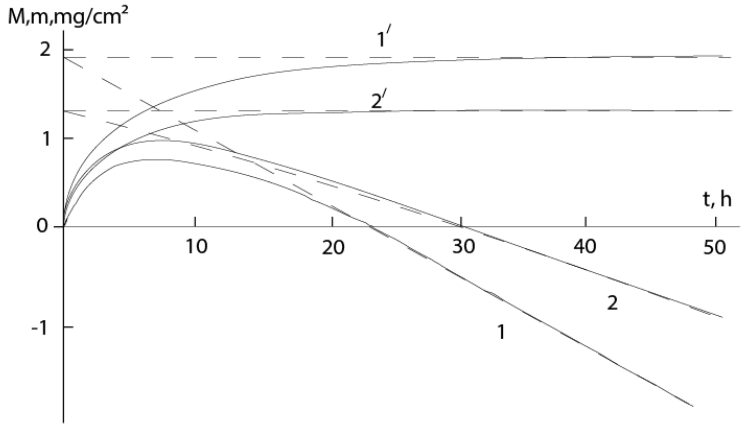

Figure 2. Kinetic curves: (1) for reaction $Cr+2HCl=CrCl_2+H_2$ at 750°C [21] and (2) $4Cr+3O_2=2CrO_3$ at 1200°C [20]; 1′,2′ – dependences m – t.

Figure 3 shows the dependence in coordinates (k_p/v_g, $\overline{M}$) for different samples from [2]. The following reactions are considered here: $2Cr+3O_2=Cr_2O_3$, $Pb+Cl_2=PbCl_2$, $Si+O_2=SiO_2$, $SiC+2O_2=SiO_2+CO_2$, $Si_3N_4+3O_2=3SiO_2+2N_2$ and $4BN+3O_2=2B_2O_3+2N_2$ (for all reactions the kinetics are parabolic: k_p - power-law constant at n=2). We have added data for reactions $Cr+2HCl=CrCl_2+H_2$ [21] and $3Ge+4NH_3=Ge_3N_4+6H_2$ [29] also with parabolic kinetics. This data fit well into this dependence (see figure).

Preprints.org (www.preprints.org) | NOT PEER-REVIEWED | Posted: 23 April 2024 doi:10.20944/preprints202404.1442.v1

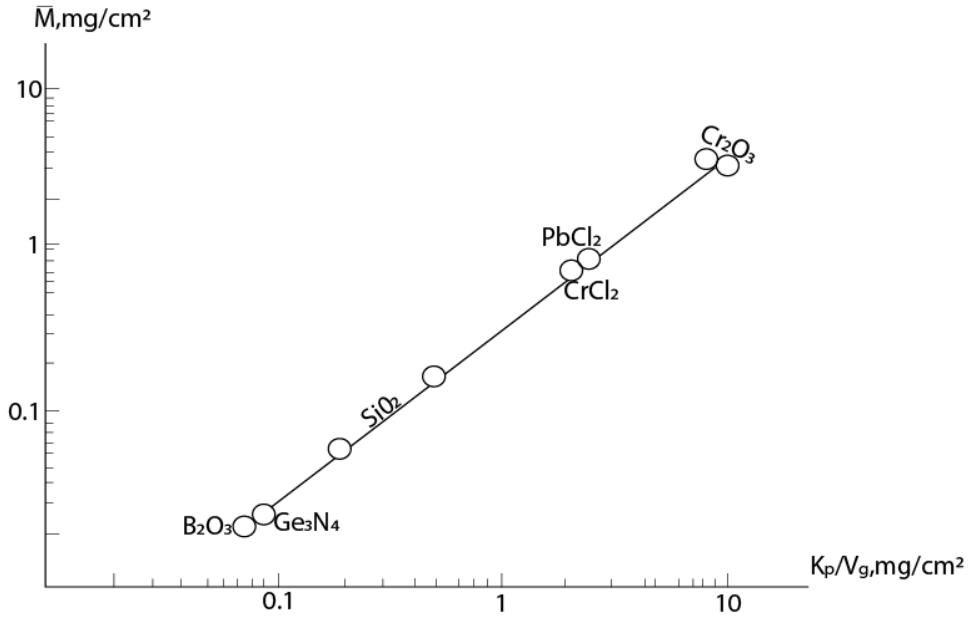

Figure 3. Dependence $\bar{M}$ – k_p/v_g for different samples.

2.2. Consideration of Preliminary Mass Reduction

In some cases the growth of scale is preceded by other processes, for example, gas etching of the surface of the metal or alloy (initial section of curve 1 in coordinate system t-W (Figure 1)). In this case, to describe the m – t dependence, it is necessary to solve the differential equation (1) with the boundary condition t = 0, m = m_0. For n=2, 3 and 4 these solutions have the form:

$$t=-(1+k)\frac{m_{max}}{v_g}\ln\frac{m_{max}-m}{m_{max}-m_0}-\frac{m-m_0}{v_g}, \quad (9)$$

$$t=(1+k)\frac{m_{max}}{2v_g}\ln\frac{(m_{max}+m)(m_{max}-m_0)}{(m_{max}-m)(m_{max}+m_0)}-\frac{m-m_0}{v_g}, \quad (10)$$

$$t=(1+k)\frac{m_{max}}{v_g}\left[\frac{1}{\sqrt{3}}\operatorname{arctg}\frac{\sqrt{3}m(m-m_0)}{m+2m_{max}}-\frac{1}{6}\ln\frac{(m_{max}-m)^2(m_0^2+m_0m_{max}+m_{max}^2)}{(m_{max}-m_0)^2(m^2+mm_{max}+m_{max}^2)}\right]-\frac{m-m_0}{v_g}, \quad (11)$$

respectively. To demonstrate, we present data on the interaction of single-crystalline Ge with NH_3+H_2O and N_2H_4 vapors (Figure 4).

 doi:10.20944/preprints202404.1442.v1

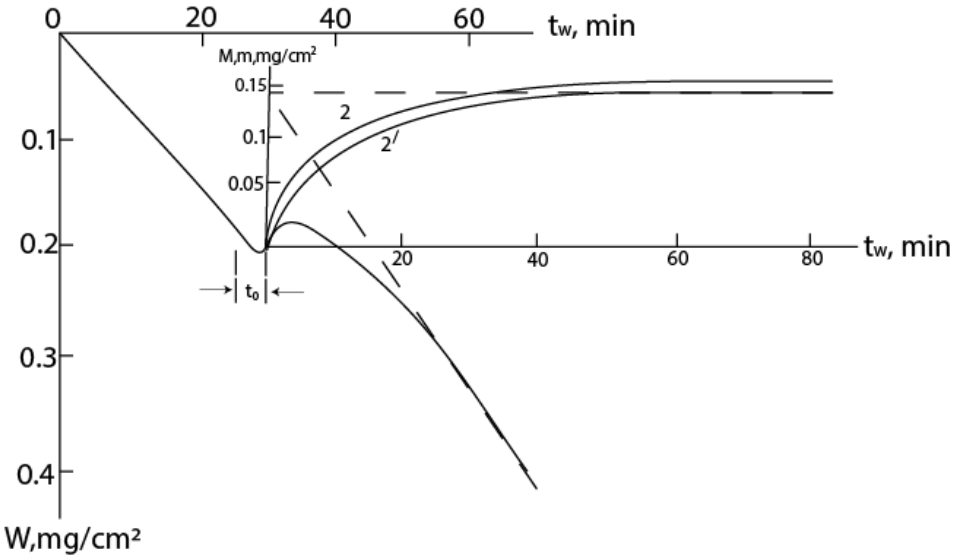

(**a**)

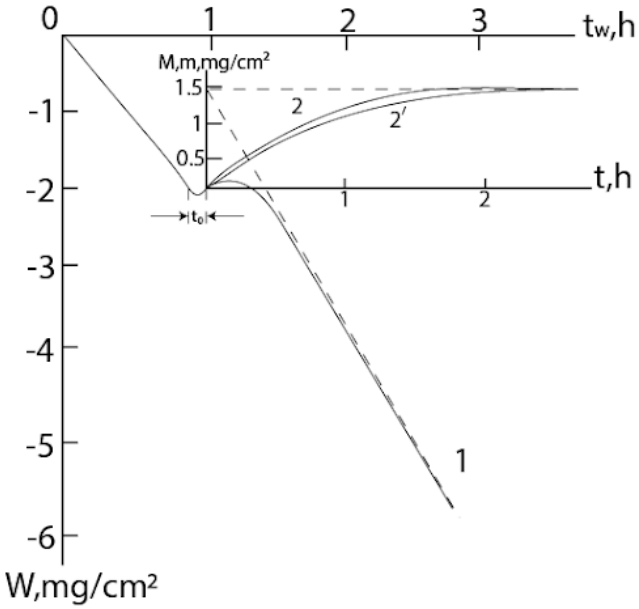

(**b**)

Preprints.org (www.preprints.org) | NOT PEER-REVIEWED | Posted: 23 April 2024 doi:10.20944/preprints202404.1442.v1

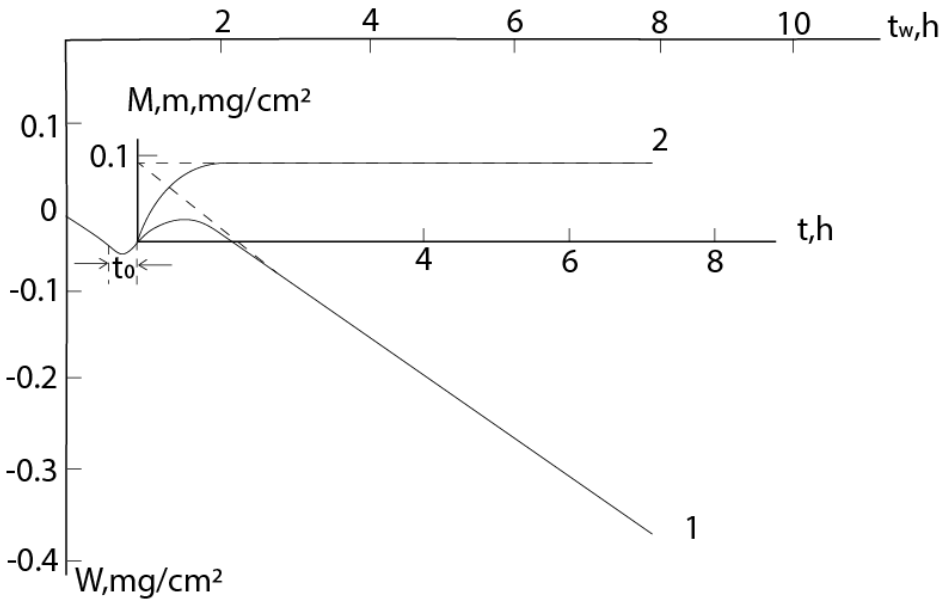

(c)

Figure 4. Kinetic dependences of interaction of Ge: with NH_3+H_2O at (**a**) P=2%, 820°C, (**b**) P=5%, 800°C, ($P \equiv P_{H2O}/P_{NH3}$); and (**c**) with N_2H_4 ($P_{N2H4}=2\cdot10^3$Pa) at 720°C – (1) dependences W – t, (2) – dependences m – t; 2′ – calculated curves (in the scale of the figure (**c**), the experimental and calculated curves practically coincide with each other). .

On these curves, the initial decrease of mass is due to the etching of the germanium surface by water vapor, which is contained in small quantities also in concentrated hydrazine (volatile GeO is formed here: $GeO+H_2O=GeO+H_2$) [30]. Also it is obvious that the formation of nitride on the germanium surface will begin before the zero point in the t - m coordinate system. But from the presented model it follows that the m - t dependences are convex in the positive direction. Time shifts between equations (3) and (9), (4) and (10), (5) and 11) are:

$$t_0=(1+k)\frac{m_{max}}{v_g}\ln\frac{m_{max}-m_0}{m_{max}}+\frac{m_0}{v_g}, \qquad (9')$$

$$t_0=(1+k)\frac{m_{max}}{2v_g}\ln\frac{m_{max}+m_0}{m_{max}-m_0}+\frac{m_0}{v_g}, \qquad (10')$$

and

$$t_0=(1+k)\frac{m_{max}}{v_g}\left[\frac{1}{6}\ln\frac{(m_{max}-m_0)^2}{m_0{}^2+m_0m_{max}+m_{max}^2}-\frac{1}{\sqrt{3}}\operatorname{arctg}\frac{\sqrt{3}m_0}{m_0+2m_{max}}\right]+\frac{m_0}{v_g}, \qquad (11')$$

respectively. Thus, the values of m_0 can be estimated by solving of transcendental equations (9′)-(11′) by substituting the values of k, m_{max}, v_g, and t_0 determined from experimental data. The main difficulty is the accurate determination of t_0 in the initial section of the curves - conducting an additional experiment of short duration would lead to even larger errors.

According to the experimental data presented in Figure 4, one can estimate $t_0\approx-3$ min, -0.14 h, and -0.33 h, respectively with Figures (a), (b) and (c). Then the values of m_0 will be ≈0.3, 0.05 and 0.03 mg/cm². As you can see, m_0 makes up (20-34)% of corresponding m_{max} (0.145, 1.42, 0.092 mg/cm², respectively) and this cannot be ignored when conducting an experiment using the gravimetric method.

 doi:10.20944/preprints202404.1442.v1

3. Conclusions

A general equation is given that describes the scale growth-evaporation kinetic (sample mass change - time) curves during the interaction of gases with the surface of metals and compounds. Special cases of parabolic, cubic and fourth degree processes are discussed. Equations are also given for the case when scale formation is preceded by the process of gas etching of the metal surface.

Acknowledgments: This review is dedicated to the memory of Dr. V.A. Arslambekov, one of the first researchers of the Tedmon's process.

Conflicts of Interest: The author declare no conflicts of interest.

Appendix

In Figure 4 the m – t dependencies are plotted according to corresponding empirical expressions of Eqs(3)-(5):

$$t \cong -3.714\ln(1-0.704m) - 2.473m \qquad (3')$$

(m – mg/cm², t – h.),

$$t \cong 34.1\ln\frac{0.145+m}{0.145-m} - 429.2m \qquad (4')$$

(m – mg/cm², t – min.)

and

$$t \cong 8.196\left[0.577\,\mathrm{arctg}\frac{1.732m}{m+0.184} - 0.167\ln\frac{(0.092-m)^2}{m^2+0.092m+0.008}\right] - 83.333m \qquad (5')$$

(m – mg/cm², t – h.). The curves constructed by these formulas are closer to the m-t curves constructed from M-t dependences with more or less accuracy (Figure 4).

References

1. Nakhutsrishvili I. Oxidation kinetics of FeCr and FeCrAl alloys: Influence of secondary processes. *Johnson Mattey Techn. Rev.*, in press.
2. Smialek J.L. (**2023**) Simplified paralinear oxidation analyses. *High Temp. Corros. Materials*, 99 (5/6) 1-27.
3. Tedmon C.S. (**1966**) The Effect of oxide volatilization on the oxidation kinetics of Cr and Fe-Cr alloys. *Electrochem. Soc.*, 113 (8) 766-768.
4. Wajszel D. (**1963**) A method for calculating paralinear constants for the formation of volatile scale. *Electrochem. Soc.*, 110 (6) 504-505.
5. Arslambekov V.A. In Book Механизм взаймодействия металлов с газами. Москва, Наука. 1966, 174 p.
6. Krejčí J., Vrtílková V., Gajdoš P. and Rada D. (**2017**) Proposal of new oxidation kinetics for sponge base E110 cladding tubes material. *Nuclear Sci. Technol.*, 3, 18.
7. Carrette F., Guinard L. and Pieraggi B. Kinetics of corrosion products release from nickel-base alloys corroding in primary water conditions. A new modeling of release, Int. Conf. Water Chemistry in Nuclear Reactor System. 2002, 22-26 April, Avignon, France, 1.
8. Stringer J. (**1972**) The functional form of rate curves for high-temperature oxidation of dispersion-containing alloys forming Cr_2O_3 scales. *Oxidat. Metals*, 5, 49-58.
9. Yong Y., Benton B.E., Howell M. and Bell G. (**2018**) High-temperature oxidation kinetics of sponge-based E110 cladding alloy. *Nucl. Materials*, 499, 595-612.
10. Smeltzer W.W., Haering R.R. and Kirkaldy J.S. (**1961**) Oxidation of metals by short circuit and lattice diffusion of oxygen. Acta Metallurgica, 9 (9) 880-885.
11. Atkinson H.V. (**1985**) A review of the role of short-circuit diffusion in the oxidation of nickel, chromium, and nickel-chromium alloys. *Oxidat. Metals*, 24, 177-197.
12. Pourbahari B. and McDermid J.R. (**2023**) Oxidation kinetics of Fe-(2-10) Mn-xSb alloys during annealing. *Materialia*, 27, 101698.
13. Feng J., Tang J., Chu M. et al. (**2022**) Effect of Cr_2O_3 on the kinetics mechanism and microstructure of pellet during oxidation roasting process. *Steel Res.*, 94 **(5)** 2200735.
14. Aghaeian S., Nourouzi F., Sloof W.G. et al. (**2023**) Predicting the parabolic growth rate constant for high-temperature oxidation of steels using machine learning models. *Corrosion Sci.*, 221, 111309.
15. Abd-El-Nabey B.A., El-Housseiny S., Abdel-Gaber A.M. and Mohamed M.E. (**2023**) Kinetics of oxidation of metals in the air at room temperature using EDX. *Results in Chem.*, 5, 100876.

 doi:10.20944/preprints202404.1442.v1

16. Estupinan-Lopez F., Orquiz-Muela C., Gaona-Tiburcio C. et al. (**2023**) Oxidation kinetics of Ti-6Al-4V alloys by conventional and electron beam additive manufacturing. *Materials*,16 (3) 1187.

17. Nakhutsrishvil, I. (**2020**) Study of growth and sublimation of germanium nitride using the concept of Tedmon's kinetic model. *Oriental J. Chem.*, 36 (5) 850-854.

18. Liu T.K. and Bautista R.G. (**1981**) Prediction of the global volatilization rate of gas-metal-alloy reaction systems—Method of calculation. *Oxidat. Metals*, 16, 243-252.

19. Jones E.S., Mosher J.F., Speiser R. and Spretnak J.W. (**1958**) Oxidation of molybdenum. *Corrosion*, 14 (1) 20-26.

20. Davis H.H., Graham H.C. and Kverens I. (**1971**) Oxidation behavior of Ni-Cr-1ThO2 alloys at 1000 and 1200°C. *Oxidat. Metals*, 3, 431-451.

21. IharaY., Ohgame H., Sakiyama K. and Hashimoto K. (**1983**) The corrosion behaviour of chromium in hydrogen chloride gas and gas mixtures of hydrogen chloride and oxygen at high temperatures. *Corrosion Sci.*, 23 (2) 167-181.

22. Smialek J. and Jacobson N.S. Oxidation of high-temperature aerospace materials, In Book: High Temperature Materials and Mechanisms, 2014, 95.

23. Nelson A.T., Sooby E.S., CimY.-J. et al. (**2014**) High temperature oxidation of molybdenum in water vapor environments. *Nucl. Materials*, 448 (1/3) 441-447.

24. Pujilaksono, B.; Jonsson, T.; Halvarsson, M. et al. Paralinear Oxidation of Chromium in O_2 + H_2O Environment at 600–700 °C. Oxidat. Metals. 2008, 70, 163

25. Wang,G.; Liu, Y.; Zhang, J. et al. Reaction of CVD BN ceramics in water vapor at 1023–1173 K using different kinetic model. Ceramic Soc. Japa.n. 2014, 12, 889

26. Kruk, A; Gil, A.; Lech, S. et al. Multiscale characterization of an oxide scale formed on the creep-resistant ATI 718Plus superalloy during high-temperature oxidation. Materials. 2021, 14, 6327

27. Dryepondt, S.N.; Pint, B.A.; Maziasz, P.J. New creep-resistant cast alloys with improved oxidation resistance in water vapor at 650–800°C. Frontniers in Materials. 2015, 2, 55

28. Peng, J.; Pillai, R.; Romedenne, M. et al. Data analytics approach to predict high-temperature cyclic oxidation kinetics of NiCr-based alloys. Materials Degradat. 2021, 5, 41

29. Nakhutsrishvili, I. Some formal aspects of Tedmon's kinetics: Growth and sublimation of Ge_3N_4. Technical Sci. & Technol. 2016, 5, 19

30. Aronishidze, M.; Nakhutsrishvili, I.; Vardosanidze, Z. et al. Some aspects of gas etching of monocrystalline germanium surface. Prooc. Georgian Acad. Sci., ser. chem. 2015, 41, 361